

This work was written as part of one of the author's official duties as an Employee of the United States Government and is therefore a work of the United States Government. In accordance with 17 U.S.C. 105, no copyright protection is available for such works under U.S. Law.

Public Domain Mark 1.0

<https://creativecommons.org/publicdomain/mark/1.0/>

Access to this work was provided by the University of Maryland, Baltimore County (UMBC) ScholarWorks@UMBC digital repository on the Maryland Shared Open Access (MD-SOAR) platform.

**Please provide feedback**

Please support the ScholarWorks@UMBC repository by emailing [scholarworks-group@umbc.edu](mailto:scholarworks-group@umbc.edu) and telling us what having access to this work means to you and why it's important to you. Thank you.

# SuperTIGER Ultra-Heavy Galactic Cosmic Ray Atmospheric Propagation Corrections and Uncertainty Analysis

**Brian F. Rauch,<sup>†,a,\*</sup> Nathan E. Walsh<sup>a</sup> and Wolfgang V. Zober<sup>a</sup> for the SuperTIGER Collaboration**

(a complete list of authors can be found at the end of the proceedings)

<sup>a</sup>*Department of Physics and McDonnell Center for the Space Sciences, Washington University,  
St. Louis, MO 63130 USA*

*E-mail:* [brauch@physics.wustl.edu](mailto:brauch@physics.wustl.edu)

The SuperTIGER (Super Trans-Iron Galactic Element Recorder) balloon-borne ultra-heavy galactic cosmic-ray (UHGCR) detector has flown twice in the stratosphere over Antarctica at altitudes up to  $\sim 130,000$  ft. Corrections for propagating through the last  $\sim 0.5\%$  of the atmosphere are based on those developed for the preceding TIGER instrument. Changes due to nuclear interactions are determined by finding top of the atmosphere (TOA) elemental abundances that yield those measured in the instrument after solving networks of equations for all elements with partial and total charge changing cross sections stepping through fine slabs of material. Varying rates of energy loss in the atmosphere for different elements yield different TOA minimum energies for the acrylic Cherenkov detector threshold ( $\sim 350$  MeV/nuc). TOA abundances corrected for nuclear interactions for each element are scaled with the fraction of the integral energy spectrum for its TOA minimum energy, using the iron spectrum for the UHGCR. Statistical uncertainties are derived at the TOA by shifting the abundance of each element individually up and down by the measured uncertainty in the instrument and calculating the TOA abundance of that element. Systematic uncertainties previously were estimated by simultaneously shifting the partial and then the total cross sections for all elements up and down by their uncertainties and finding TOA abundances compared to the nominal values. Here we present a Monte Carlo study of the systematic impact of simultaneously randomly varying atmospheric propagation parameters over many trials to find the normal range of variation in the resulting TOA element abundances. Total and partial charge changing cross sections for each element are individually varied in each sampling.

*37<sup>th</sup> International Cosmic Ray Conference (ICRC 2021)*

*July 12th – 23rd, 2021*

*Online – Berlin, Germany*

---

\*Presenter

<sup>†</sup>SuperTIGER supported by NASA under grant numbers NNX09AC17G, NNX14AB25G, NNX15AC23G, and 80NSSC20K0405 and the Peggy and Steve Fossett Foundation

## 1. Introduction

The best measurements of the ultra-heavy Galactic cosmic rays (UHGCR),  $_{30}\text{Zn}$  and higher charge elements, with single-element resolution to-date have been made by the balloon-borne Super Trans-Iron Galactic Recorder (SuperTIGER) instrument [1–4] that is over four times the size of the predecessor TIGER instrument [5–7]. The advantage of balloon instruments is the larger geometric acceptances that can be flown than on space missions, but balloon-altitude measurements must be corrected for propagation through the residual atmosphere above the balloon. These corrections include those for nuclear interactions and energy losses in the instrument and atmosphere to derive top of the atmosphere (TOA) elemental abundances. SuperTIGER is nearly as large an UHGCR detector as can be flown on existing stratospheric balloons, and there is tension between detector size and weight versus higher altitude and reduced atmospheric overburden.

The UHGCR provide insight into the origins of the Galactic cosmic rays (GCR), how they are accelerated, and the nucleosynthetic sources of the heavy elements. In Fig 1, the relative abundances of elements from  $_{1}\text{H}$  to  $_{40}\text{Zr}$  for GCR with energies of 2 GeV/nucleon are compared with the Solar System (SS) abundances [8] normalized to  $_{14}\text{Si}$ . These two samples of galactic matter are nominally consistent, with most of the differences accounted for through both cosmic ray spallation between the source and detection and by acceleration efficiencies. In the GCR we see that  $_{26}\text{Fe}$  is  $\sim 5 \times 10^3$  times less abundant than  $_{1}\text{H}$ , the UHGCR from  $_{30}\text{Zn}$  to  $_{40}\text{Zr}$  are  $\sim 10^5$  times less abundant than  $_{26}\text{Fe}$ , and the heavier UHGCR are even more scarce still.

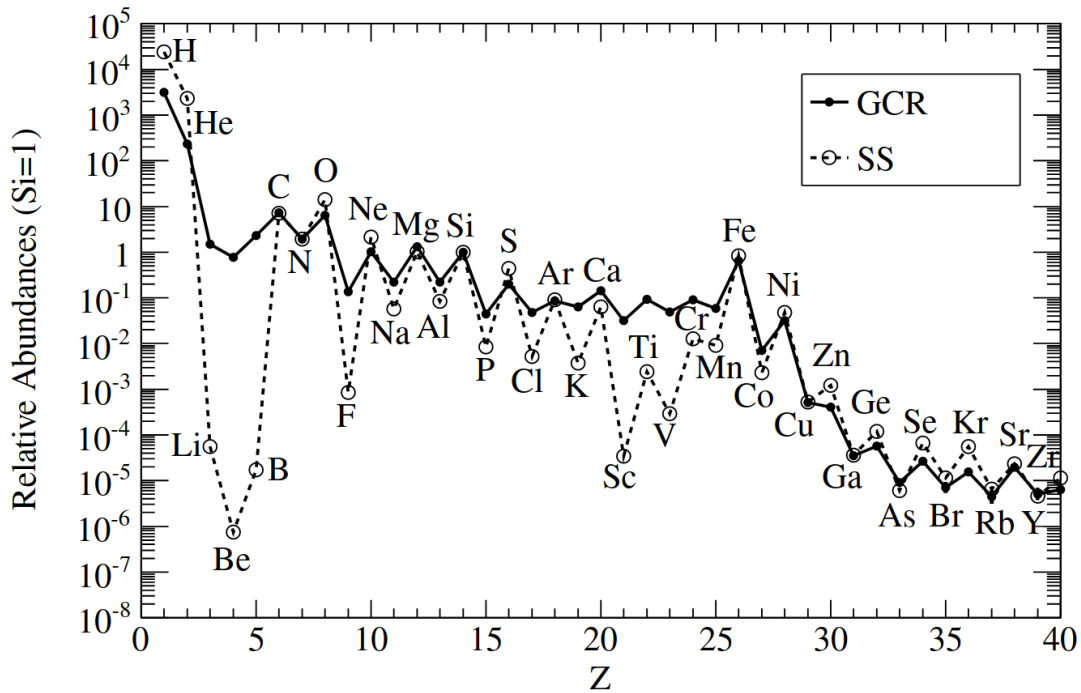
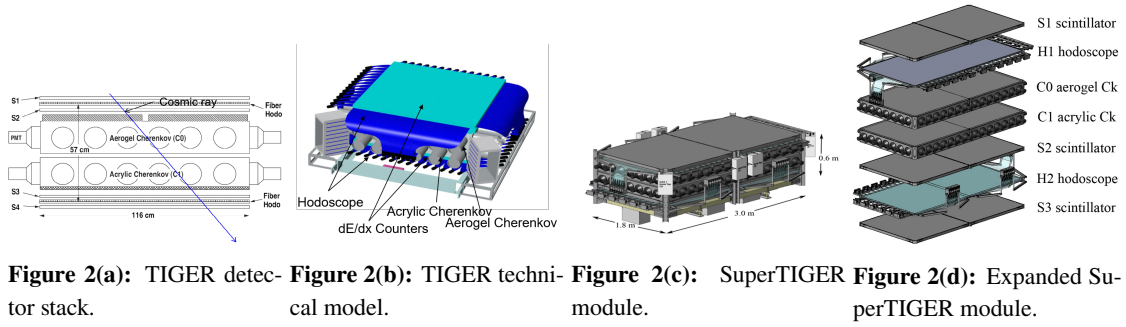


**Figure 1:** Solar System (SS) [8] and Galactic cosmic-ray (GCR) relative abundances at 2 GeV/nuc. GCR data is sourced for  $1 \leq Z \leq 2$  from [9],  $Z=3$  from [10],  $4 \leq Z \leq 28$  from [11],  $Z=29$  from [7], and  $28 \leq Z \leq 40$  from [2] and normalized to  $_{14}\text{Si}$ .

## 2. TIGER and SuperTIGER

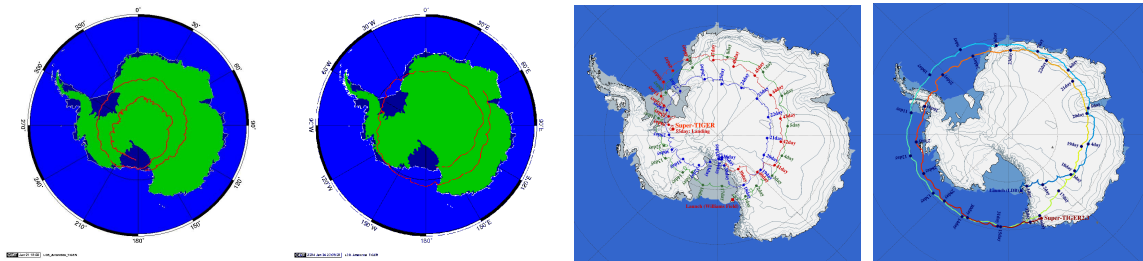
### 2.1 Instruments

SuperTIGER is a supersized ( $\sim 4\times$ ) version of the predecessor TIGER instrument. TIGER, shown in a side view in Fig. 2a and in a technical model in Fig. 2b, was a 1.16 m square 0.57 m tall stack of four compact wavelength-shifter readout scintillator detectors sandwiching scintillating optical fiber hodoscopes above and below aerogel and acrylic Cherenkov light collection box detectors. One of two SuperTIGER modules is shown in Fig. 2c and in an expanded view in Fig. 2d, which is like two TIGER detectors connected together. SuperTIGER differs from TIGER in having only one scintillator at the top of the stack above the Cherenkov detectors to reduce the material in the GCR beam.



### 2.2 Flights

TIGER and SuperTIGER each had two successful Antarctic flights: TIGER 2001 from December 21, 2001 – January 21, 2002 for 32 days with  $3.7\times 10^5$   $^{26}\text{Fe}$  shown in Fig. 3a, TIGER 2003 from December 27, 2003 – January 4, 2004 for 18 days with  $2.5\times 10^5$   $^{26}\text{Fe}$  shown in Fig. 3b, SuperTIGER 2012 from December 8, 2012 - February 1, 2013 for 55 days with  $5.38\times 10^6$   $^{26}\text{Fe}$  shown in 3c, and SuperTIGER 2019 from December 15, 2019 - January 17 2020 for 32 days with  $1.3\times 10^6$   $^{26}\text{Fe}$  shown in Fig 3d, where the UHGCR statistics scale with  $^{26}\text{Fe}$ . The first TIGER and SuperTIGER flights set duration records for zero-pressure heavy-lift stratospheric balloons, with the SuperTIGER record still standing.



### 2.3 Altitude Profiles

The 2001 and 2003 TIGER flights had very different altitude profiles because the 2001 flight had a leaky balloon. The 2001 altitude profile in Fig. 4a has a steadily decreasing trend superposed on the normal diurnal altitude variations except for two significant rises associated with ballast drops, while the 2003 altitude in Fig. 4b varies around a stable, higher altitude.

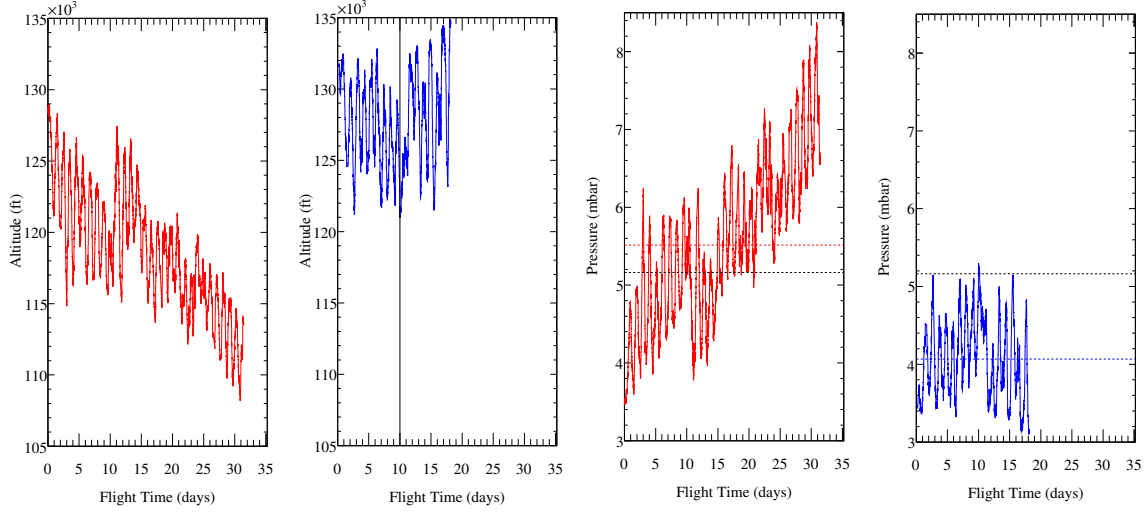


**Figure 4(a):** TIGER 2001 altitude profile. **Figure 4(b):** TIGER 2003 altitude profile. **Figure 4(c):** TIGER 2001 pressure profile. **Figure 4(d):** TIGER 2003 pressure profile.

Due to the limited statistics of the observed UHGCR the atmospheric propagation corrections for TIGER [6, 7] and SuperTIGER [1–3] have been performed with a mean overburden. The average overburden for events in the TIGER analysis from both flights (5.16 mbar) is shown by the black dashed line in Fig. 4c for the 2001 and Fig. 4d for the 2003 flight, with the red and blue dashed lines giving the mean overburdens for the 2001 (5.5 mbar) and 2003 (4.1 mbar) flights, respectively. The atmospheric corrections use the weighted average of the overburdens from the two flights (5.0 mbar), which was then converted to areal density and multiplied by the average of the secant of the incidence angle ( $\langle \sec(\theta) \rangle = 1.245$ ) to get the mean atmospheric depth 6.22 g/cm<sup>2</sup>.

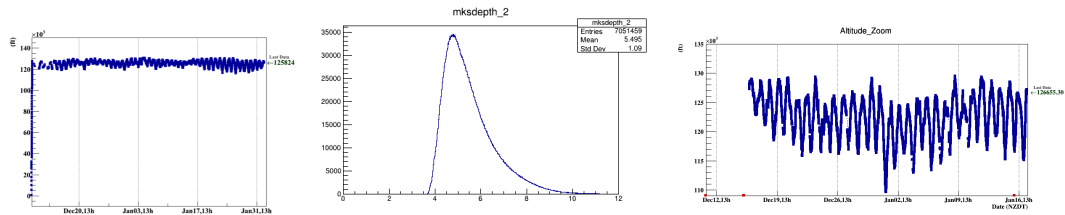


**Figure 5(a):** SuperTIGER 2012 altitude profile. **Figure 5(b):** SuperTIGER 2012 atmospheric overburden distribution. **Figure 5(c):** SuperTIGER 2019 altitude profile at float.

The 2019 SuperTIGER flight took a much more northerly route than previous flights and spent a lot of time over the ocean where there is less albedo that led to the lower altitude profile shown in Fig. 5c compared to that for the 2012 flight shown in Fig. 5a. The histogram of the 2012 SuperTIGER flight atmospheric overburden profile is shown in Fig. 8b, which gives a mean

atmospheric depth for this flight of  $5.50 \text{ g/cm}^2$  with a standard deviation  $\sigma=1.09 \text{ g/cm}^2$ . The data from the 2019 SuperTIGER flight have not yet been analyzed through atmospheric propagation corrections, but the average vertical overburden was  $\sim 5.2 \text{ mbar}$ .

### 3. Atmospheric Propagation Corrections

To compare GCR abundances measured in the instrument with measurements in space it is necessary to first correct the abundances for the interactions and energy losses as particles travel down through the atmosphere and within the instrument. Corrections are first made for the propagation in the instrument, and the material above the first charge detector (top scintillator) must be handled differently from that in the active region where interacting particles can be identified. The material at the top of the instrument is included in the atmospheric corrections that account for both loss and gain of each element through nuclear interactions, while within the active area of the detector only corrections for loss are made since interaction cuts have been applied. The inactive material above the top scintillator detectors was modeled with an equivalent depth of atmosphere in the propagation corrections, with  $1.31 \text{ g/cm}^2$  for TIGER and  $0.1 \text{ g/cm}^2$  for SuperTIGER based on the material above the top scintillator given in Table 2. Nuclear interaction probabilities and the rate of energy loss both increase for nuclei with higher  $Z$ , where energy loss increases as  $Z^2$  and interactions proportional increases with nuclear cross sectional area  $\sim A^{2/3}$ , where  $A \propto Z$ . The total charge changing cross sections are given in Fig. 6a for the materials used in the atmospheric and instrument propagation corrections, showing the increase in the cross sections is clearly less than linear in  $Z$ .

TIGER and SuperTIGER cannot discriminate between isotopes, so the interactions considered in the atmospheric and instrument propagation corrections are total and partial charge changing cross sections. The total charge changing cross sections account for losses of an element, while the partial charge changing cross sections determine when a higher  $Z$  particle will interact into a given element. In the atmosphere and top instrument material, the correction process tracks the changes that will add to the flux of each element and that will reduce it, and the observed flux of each element depends on the fluxes of all elements that can transform into it and the cross sections for these changes, which depend on the material the particles are passing through.

The total charge changing cross sections are given by  $\sigma_{tot}(P, T) = \pi[R_P + R_T - (3.20 \pm 0.05)]^2$ , where  $P$  and  $T$  refer to the projectile and target nuclei, and  $R_P$  and  $R_T$  are their respective nuclear radii [12]. The partial charge changing cross section is given by

$$\sigma_{\Delta Z}(A_P, A_T, K, \Delta Z) = p_1(A_P^{1/3} + A_T^{1/3} - p_2)(1 + p_3/K)|\Delta Z|^{-p_4[1+A_P^{1/3}/p_5+A_T^{1/3}/p_6+p_7/K]}, \quad (1)$$

where  $A_P$  and  $A_T$  are the atomic masses of the projectile and target nuclei,  $\Delta Z$  is the change in charge of the projectile,  $K$  is the total kinetic energy of the projectile, and the parameters are given

parameter	value
$p_1$	$21.2 \pm 0.5 \text{ mb}$
$p_2$	$1.08 \pm 0.15$
$p_3$	$(0.485 \pm 0.014)A \text{ GeV}$
$p_4$	$0.094 \pm 0.013$
$p_5$	$1.11 \pm 0.02$
$p_6$	$10.8 \pm 1.6$
$p_7$	$(0.85 \pm 0.03)A \text{ GeV}$
$\chi^2_\nu$	2.84
$N$	1741

**Table 1:** Partial charge changing cross section parameters taken from Table VIII in the paper [12].

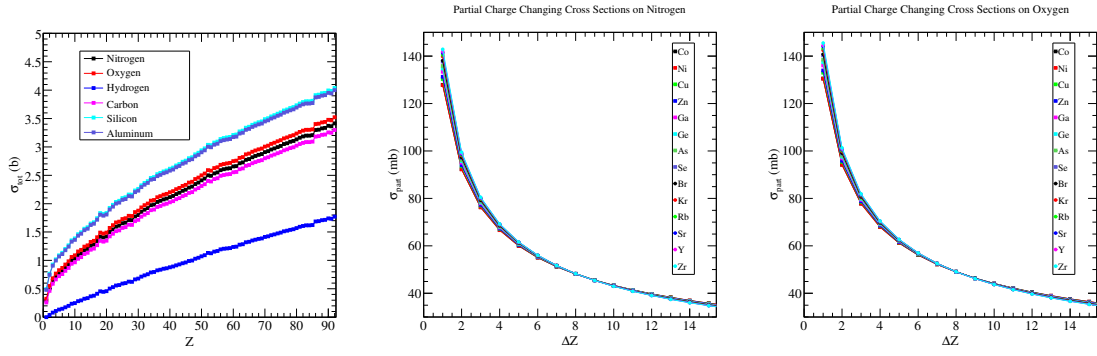


**Figure 6(a):** Total charge changing cross sections. **Figure 6(b):** Partial charge changing cross sections for  $^{14}\text{N}$  **Figure 6(c):** Partial charge changing cross sections for  $^{16}\text{O}$

in Table 1. For this analysis a value of  $K = 2A$  GeV was selected as representative for the TIGER GCR and  $K = 3.1A$  GeV was chosen for the SuperTIGER GCR. The partial charge changing cross sections for the projectile elements from  $^{28}\text{Ni}$  to  $^{40}\text{Zr}$  for the atmospheric gas targets of  $^{7}\text{N}$  and  $^{8}\text{O}$  are shown in Fig. 6b and Fig. 6c, respectively.

The measured abundances are corrected to the top detector for interaction losses in the active instrument area in TIGER [5–7] and SuperTIGER [1–3]. Corrections for the inactive detector material above the middle of the top scintillator radiator in TIGER and SuperTIGER listed in Table 2 were folded into the corrections for interactions in the atmosphere. The top insulation for SuperTIGER is melamine ( $\text{C}_3\text{H}_6\text{N}_6$ ) foam, but foam is polymerized malamine sodiumbisulfide ( $\text{C}_9\text{H}_6\text{Na}_6\text{S}_6\text{O}_{18}$ ), which I presume loses H in polymer linkages, at least two per molecule to form a strand and more for cross linkages. To date this material has been approximated as acrylic.

detector material	chemical formula	TIGER top	TIGER active	ST top	ST active
PET	$\text{C}_{10}\text{H}_8\text{O}_4$	0.102	0	0.025	0.062
PMMA	$\text{C}_5\text{H}_8\text{O}_2$	0	0.938	0.040	1.499
aluminum	Al	0.148	0.07	0.033	0.372
PS	$\text{C}_8\text{H}_8$	0.342	1.920	0	0.388
PVT	$\text{C}_9\text{H}_{10}$	0.412	1.442	0.523	1.057
silica	$\text{SiO}_2$	0	0.586	0	0.614

**Table 2:** TIGER and SuperTIGER instrument materials above middle of first scintillator detector (top) and in average in the active area (active) in  $\text{g/cm}^2$ : polyethylene terephthalate (PET) - Mylar, polymethyl methacrylate (PMMA) - acrylic, aluminum (Al), polystyrene (PS), polyvinyltoluene (PVT), silica  $\text{SiO}_2$ .

A correction for energy losses is made by calculating the minimum energy at the top of the atmosphere required to be above threshold in the acrylic Cherenkov detector based on the average energy losses in detector materials and the atmosphere. The top of the atmosphere abundances corrected for interactions in the atmosphere are then renormalized compared to iron based on evaluating the normalized integral spectrum of each element derived from differential spectra [13] for elements below  $^{26}\text{Ni}$  and scaled  $^{26}\text{Fe}$  spectra for UHGCR.



## 4. Results and Discussion

Correcting for cosmic-ray nuclear interactions and energy losses in the atmosphere is particularly difficult for ultra-heavy cosmic rays where statistics are very limited, which requires aggregating all of the data to make average corrections. I show the magnitude of the TIGER atmospheric interaction corrections in Fig. 7a and with the energy correction added in Fig. 7b. Sensitivity studies for the interaction corrections find that the results are more sensitive to variations in the atmospheric overburden shown in Fig. 7c than in the assumed cross section energy shown in Fig. 7d.

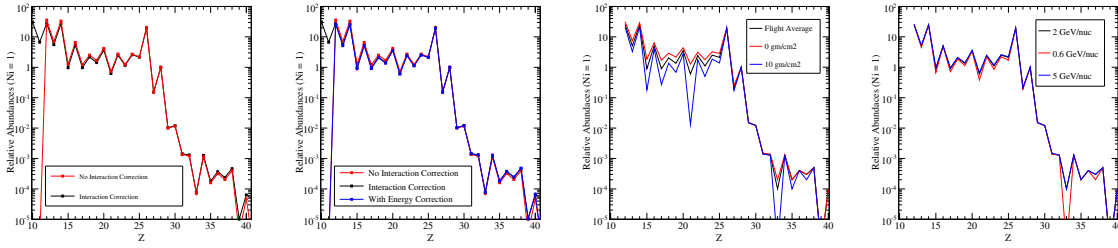


**Figure 7(a):** Impact of atmospheric interaction corrections on TIGER abundances. **Figure 7(b):** Impact of interaction corrections with energy loss correction on TIGER TOA abundances. **Figure 7(c):** Sensitivity of TIGER TOA abundances to atmospheric depth. **Figure 7(d):** Sensitivity of TIGER TOA abundances to interaction cross section energy.

Atmospheric interaction corrections for SuperTIGER are shown in Fig. 8a compared with SS abundances. The TOA abundances include statistical and systematic uncertainties, the former found by shifting instrument abundances up and down by their statistical uncertainties and calculating TOA abundances, and the latter by globally shifting the cross sections up and down by their uncertainties. SuperTIGER sensitivity studies also found that the corrections depend most strongly on the atmospheric depth assumed, as shown in Fig. 3d showing depth shifted by  $\pm 1\sigma$  and  $\pm 2\sigma$ .

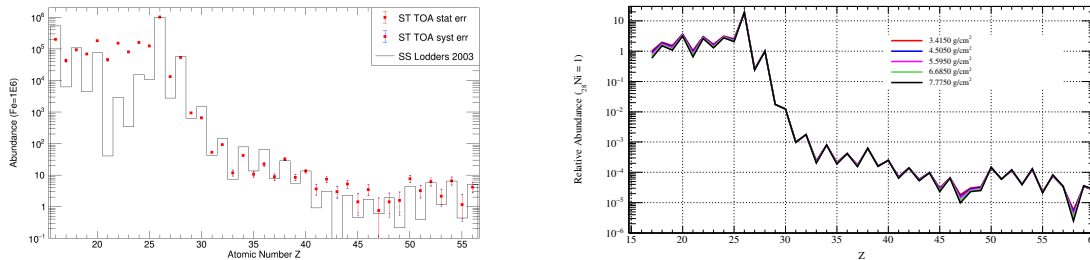


**Figure 8(a):** SuperTIGER 2012 TOA relative abundances with systematic error bars based on scaling cross sections up and down by their uncertainties. **Figure 8(b):** SuperTIGER 2012 atmospheric propagation correction dependence on assumed depth.

There are a number of improvements we plan to make to the SuperTIGER atmospheric corrections in the near future. First, we will update the energy-loss corrections to include elements from  $_{41}\text{Nb}$  to  $_{56}\text{Ba}$  that are presently extrapolated from elements  $_{40}\text{Zr}$  and lighter. We will use a more detailed model of material composition in energy loss and nuclear interaction models rather than the aggregated approach and similar materials approximation used to date. An updated version of the atmospheric propagation code will find the TOA abundances that result in the instrument



abundances instead of the TOA relative abundances that yield those at the instrument. Finally, we will complete the promised Monte Carlo study of the systematics of varying the major atmospheric propagation parameters and the cross section parameters within their ranges.

### Acknowledgements

The material contained in this document is based upon work supported by a National Aeronautics and Space Administration (NASA) grant or cooperative agreement. Any opinions, findings, conclusions, or recommendations expressed in this material are those of the author and do not necessarily reflect the views of NASA.

### 5. References

- [1] R. P. Murphy, *Identifying the Origin of Galactic Cosmic Rays with the SuperTIGER Instrument*. PhD thesis, Washington University in St. Louis, 2015.
- [2] R. P. Murphy *et al.*, “Galactic Cosmic Rays Origins and OB Associations: Evidence from SuperTIGER Observations of Elements  $^{26}\text{Fe}$  through  $^{40}\text{Zr}$ ,” *The Astrophysical Journal*, vol. 831, no. 2, p. 148, 2016.
- [3] N. E. Walsh, *SuperTIGER Elemental Abundances for the Charge Range  $41 \leq Z \leq 56$* . PhD thesis, Washington University in St. Louis, 2020.
- [4] N. E. Walsh *et al.*, “SuperTIGER Abundances of Galactic Cosmic Rays for the Atomic Number (Z) Interval 30 to 56,” in *Proceedings of 37th International Cosmic Ray Conference — PoS(ICRC2021)*, vol. 395, p. 118, 2021.
- [5] J. T. Link, *Measurements of Ultra-Heavy Galactic Cosmic Rays with the TIGER Instrument*. PhD thesis, Washington University in St. Louis, 2003.
- [6] B. F. Rauch, *Measurement of the Relative Abundances of the Ultra-Heavy Galactic Cosmic Rays ( $30 \leq Z \leq 40$ ) with the Trans-Iron Galactic Element Recorder (TIGER) Instrument*. PhD thesis, Washington University in St. Louis, 2008.
- [7] B. F. Rauch *et al.*, “Cosmic Ray Origin in OB Associations and Preferential Acceleration of Refractory Elements: Evidence from Abundances of Elements  $^{26}\text{Fe}$  through  $^{34}\text{Se}$ ,” *The Astrophysical Journal*, vol. 697, no. 2, pp. 2083–2088, 2009.
- [8] K. Lodders, “Solar System Abundances and Condensation Temperatures of the Elements,” *The Astrophysical Journal*, vol. 519, pp. 1220–1247, 2003.
- [9] T. Sanuki *et al.*, “Precise Measurement of Cosmic-Ray Proton and Helium Spectra with the BESS Spectrometer,” *The Astrophysical Journal*, vol. 545, no. 2, pp. 1135–1142, 2000.
- [10] M. Aguilar *et al.*, “Isotopic Composition of Light Nuclei in Cosmic Rays: Results from AMS-01,” *The Astrophysical Journal*, vol. 736, p. 105, Aug. 2011.
- [11] J. J. Engelmann *et al.*, “Charge Composition and Energy Spectra of Cosmic-Ray Nuclei for Elements from Be to Ni. Results from HEAO-3-C2,” *Astronomy & Astrophysics*, vol. 233, pp. 96–111, 1990.
- [12] B. S. Nilsen *et al.*, “Fragmentation Cross Sections of Relativistic  $^{84}_{36}\text{Kr}$  and  $^{109}_{47}\text{Ag}$  Nuclei in Targets From Hydrogen to Lead,” *Physical Review C*, vol. 52, no. 6, pp. 3277–3290, 1995.
- [13] J. S. George *et al.*, “Elemental Composition and Energy Spectra of Galactic Cosmic Rays During Solar Cycle 23,” *The Astrophysical Journal*, vol. 698, no. 2, 2009.

**Full Authors List: SuperTIGER Collaboration**

Y. Akaïke<sup>1</sup>, W. R. Binns<sup>2</sup>, R. G. Bose<sup>2</sup>, T. J. Brandt<sup>3</sup>, D. Braun<sup>2</sup>, N. Cannady<sup>4,5,6</sup>, P. F. Dowkontt<sup>2</sup>, T. Hams<sup>4,5,6</sup>, M. H. Israel<sup>2</sup>, J. F. Krizmanic<sup>4,5,6</sup>, A. W. Labrador<sup>7</sup>, J. T. Link<sup>4,5,6,‡</sup>, R. A. Mewaldt<sup>7</sup>, J. W. Mitchell<sup>5</sup>, R. P. Murphy<sup>2</sup>, G. A. de Nolfo<sup>8</sup>, B. F. Rauch<sup>2</sup>, K. Sakai<sup>4,5,6</sup>, M. Sasaki<sup>5,6,9</sup>, G. Simburger<sup>2</sup>, E. C. Stone<sup>7</sup>, T. Tatoli<sup>8,10</sup>, N. E. Walsh<sup>2</sup>, J. E. Ward<sup>2</sup>, M. E. Wiedenbeck<sup>11,7</sup>, and W. V. Zober<sup>2</sup>

<sup>1</sup>Waseda Research Institute for Science and Engineering, Waseda University, Tokyo 162-0044, Japan

<sup>2</sup>Department of Physics and McDonnell Center for the Space Sciences, Washington University, St. Louis, MO 63130-4899, USA

<sup>3</sup>NASA Goddard Space Flight Center, Greenbelt, MD 20771, USA

<sup>4</sup>Center for Space Sciences and Technology, University of Maryland Baltimore County, Baltimore, MD 21250, USA

<sup>5</sup>Astroparticle Physics Laboratory, NASA/GSFC, Greenbelt, Maryland 20771, USA

<sup>6</sup>Center for Research and Exploration in Space Sciences and Technology, NASA/GSFC, Greenbelt, MD 20771, USA

<sup>7</sup>California Institute of Technology, Pasadena, CA 91125, USA

<sup>8</sup>Heliospheric Physics Laboratory, NASA/GSFC, Greenbelt, Maryland 20771, USA

<sup>9</sup>Department of Astronomy, University of Maryland, College Park, Maryland 20742, USA

<sup>10</sup>Department of Physics, Catholic University of America, Washington, DC 20064, USA

<sup>11</sup>Jet Propulsion Laboratory, Pasadena, CA 91109, USA

<sup>‡</sup>As of May 21, 2021 this person is no longer associated with NASA or CRESST